Journal of Solid State Chemistry 181 (2008) 1307–1313

Contents lists available at ScienceDirect

Journal of Solid State Chemistry

journal homepage: www.elsevier.com/locate/jssc

Formation mechanism and luminescence appearance of Mn-doped zinc silicate particles synthesized in supercritical water

Masafumi Takesue [a,b], Atsuko Suino [c], Yukiya Hakuta [c], Hiromichi Hayashi [c], Richard Lee Smith Jr.[a,*]

[a] Research Center of Supercritical Fluid Technology, Tohoku University, 6-6-11, Aramaki Aza Aoba, Aoba-ku, Sendai 980-8579, Japan
[b] Research and Development Center, Bando Chemical Industries, Ltd., 4-6-6, Minatojima Minamimachi, Chuo-ku, Kobe 650-0047, Japan
[c] Research Center for Compact Chemical Process, National Institute of Advanced Industrial Science and Technology, 4-2-1, Nigatake, Miyagino-ku, Sendai 983-8551, Japan

ARTICLE INFO

Article history:
Received 26 January 2008
Received in revised form
27 February 2008
Accepted 28 February 2008
Available online 6 March 2008

Keywords:
Supercritical water
Hydrothermal reaction
Low-temperature process
Phase formation
Luminescence appearance
Inorganic phosphor

ABSTRACT

Luminescence appearance of Mn-doped zinc silicate (Zn_2SiO_4:Mn^{2+}, ZSM) formed in supercritical water at 400 °C and 29 MPa at reaction times from 1 to 4320 min was studied in the relation to its phase formation mechanism. Appearance of luminescent ZSM from green emission by α-ZSM and yellow emission by β-ZSM occurred over the same time period during the onset of phase formation at a reaction time of 2 min. Luminescence appeared at a much lower temperature and at shorter reaction times than the conventional solid-state reaction. Needle-like-shaped α-ZSM was the most stable particle shape and phase in the supercritical water reaction environment and particles formed via two routes: a homogenous nucleation route and a heterogenous route that involves solid-state diffusion and recrystallization.

1. Introduction

Processing technologies for materials, especially those using supercritical water and hydrothermal conditions have been investigated extensively for inorganic materials containing phosphors [1–3]. Such hydrothermal processes have mainly attracted the attention of researchers aimed at producing nanoparticles. However, hydrothermal reactions in supercritical water have the potential for producing highly crystalline inorganic materials.

Presently, commercial inorganic phosphors are synthesized by conventional solid-state reaction processes [4]. In the solid-state reaction, phase formation of phosphors proceeds by solid-state diffusion among solid starting materials, whose diffusion rates are very low. Therefore, commercial inorganic phosphors are usually synthesized at reaction temperatures higher than 1000 °C and for reaction times of several hours or more to produce phosphors that have high crystallinity and high luminescence. On the other hand, synthesis at supercritical conditions has the potential to obtain highly crystalline and highly luminescent phosphors at lower temperatures and shorter times than those used in the solid-state reaction process, since reaction rates tend to be greatly accelerated in supercritical water and the solvent properties such as density of water can be varied with temperature or pressure. A low-temperature process (ca. 400 °C) that could overcome the limitations of solid-state diffusion would bring a large benefit to industry and help to solve both environmental and energy problems. Even though the conventional hydrothermal process can provide a low-temperature route to produce commercial phosphor, however, it is not being used on a practical scale, most likely due to the low crystallinity and therefore the low luminescence of the formed materials. In this respect, it is especially important to understand the phase formation mechanism and crystal structure for achieving highly luminescent phosphors in water at high temperatures and high pressures.

Mn-doped zinc silicate (Zn_2SiO_4:Mn^{2+}, ZSM) is a green emitting phosphor excited by electron beam or ultraviolet light [4,5] and has been in practical use since the 1930s, where it is used in most advanced plasma displays [4,6,7]. Zinc silicates have potential as materials for multi-color emitting phosphors by changing the dopant ion, for example, red emission by Eu^{3+} [8–11], blue emission by Eu^{2+} [12] and Ce^{3+} [13], and an additional green emission by Tb^{3+} [13,14]. ZSM and zinc silicates have received considerable attention not only as phosphor materials, but also as typical materials in processing research by a variety of methods [4,6,15–17]. Although, synthesis of ZSM has been widely studied with hydrothermal [5,18–23], and solvothermal [24] processing, the luminescence of ZSM produced by these methods

* Corresponding author at: Research Center of Supercritical Fluid Technology, Tohoku University, 6-6-11, Aramaki Aza Aoba, Aoba-ku, Sendai 980-8579, Japan. Fax: +81 22 795 5864.
E-mail address: smith@scf.che.tohoku.ac.jp (R.L. Smith Jr.).

0022-4596/$ - see front matter © 2008 Elsevier Inc. All rights reserved.
doi:10.1016/j.jssc.2008.02.036

is much lower than that produced by solid-state reactions [20]. Therefore, it can be said that the phase formation mechanism of ZSM under hydrothermal conditions is still not understood well in the relationship with the luminescent properties, and further investigation is necessary to produce luminescent materials that have high crystallinity on a practical scale.

We previously studied the dissolution behavior of ZSM precursors and particle formation of ZSM in supercritical water by *in situ* observations with a hydrothermal diamond anvil cell (HDAC). In that work, we found that needle-like-shaped ZSM formed thorough homogeneous nucleation in water close to the critical point of water [25]. In this work, we examine the time evolution of the luminescence appearance and relate this to the phase formation mechanism.

2. Experimental

2.1. Materials and precursor preparation

Zinc oxalate dihydrate ($ZnC_2O_4 \cdot 2H_2O$, Kojundo Chemical Laboratory, 99.9%), manganese oxalate (MnC_2O_4, Kojundo Chemical Laboratory, 99.9%), and spherical silica particles (amorphous SiO_2, Nippon Shokubai KE-P50, mean particle diameter, 500 nm) were used as raw materials. Net SiO_2 content in the silica particles was 84.9 wt% as determined by measuring weight loss with thermogravimetric analysis. The water used was deionized water. Precursors were prepared by adequately mixing raw materials for about 30 min with an agate mortar and an agate pestle, where the Zn/Mn/Si molar ratio was 1.96/0.04/1 and thus the Mn content was 2 mol% in all experiments.

2.2. ZSM preparation in supercritical water

ZSM was produced at supercritical conditions with batch reactors made of stainless steel SUS 316 (10 mL volume). Reactions were carried out at conditions to give theoretical concentrations of ZSM of 0.075–0.60 mol/kg. Water density in the batch reactor was 0.3 g/cm^3 to give a calculated pressure of 29 MPa at the reaction temperature of 400 °C. Methods for the calculation of pressure are given in the literature [26,27]. The batch reactors were heated in a molten salt bath at the given temperature (400 °C) and time (1–4320 min) and quenched in water at room temperature. Temperature inside the batch reactor was measured by a K-type thermocouple inserted into the reactor. Heat-up time required was roughly between 50 s (374 °C) and 120 s (400 °C) to reach the desired temperature with a molten salt bath. After cooling and opening the reactor, solid product was separated from the liquid by filtering with 0.1 μm membrane filters and washed several times with deionized water. The product was dried for 24 h at 60 °C in an electric oven.

2.3. Analyses

The crystalline phase was characterized by the X-ray powder diffractometry (XRD) patterns using a Rigaku RINT2000 equipped with graphite monochromatized Cu$K\alpha$ radiation. The morphology was evaluated with scanning electron microscopy (SEM), using a JEOL JSM-5600LV at an accelerating voltage of 15–20 keV. Vacuum ultraviolet photoluminescence (VUV-PL) emission spectra were measured in a vacuum chamber equipped with a rotary pump at pressure of about 7 Pa and at room temperature. Product materials were placed into round shaped holders whose diameter was 26 mm and depth was 0.2 mm and were irradiated in a vertical orientation with a deuterium lamp, Hamamatsu Photonics L8998 (peak wavelength of emission, 161 nm) and power supply, Hamamatsu Photonics C9598. Emission was detected at a direction 45° to that of the sample with optical fibers and a photonic multichannel analyzer, Hamamatsu Photonics PMA-11. The color coordinates were calculated by using spectra observed from 380 to 780 nm and the CIE (Commission Internationale de l'Eclairage) 1931 standard colorimetric observer data (visual angle, 2°). Weight losses were measured with thermogravimetric analysis (TGA), using a Bruker AXS TG-DTA 2010SA at a heating rate of 10 °C/min to 1000 °C in N_2 atmosphere (100 mL/min). The products were dissolved in 1 M nitric acid. The elemental contents were measured with inductively coupled plasma atomic emission spectrometry (ICP-AES) (Seiko instruments SPS7800).

3. Results and discussion

3.1. Phase formation mechanism of Mn-doped zinc silicate in supercritical water

Analysis of products at various conditions is summarized in Table 1. The precursor is expected to react theoretically as follows:

$$1.96ZnC_2O_4 \cdot 2H_2O + 0.04MnC_2O_4 + SiO_2 + 2H_2O = Zn_{1.96}Mn_{0.04}SiO_4 + 4CO_2 + 2H_2 + 3.92H_2O \quad (1)$$

The elementary process in reaction (1) can be expressed by Eqs. (2)–(5) as follows, assuming ionization to some extent of each of the starting materials:

$$SiO_{2(solid)} + 2H_2O = 4H^+{}_{(aq)} + SiO_4{}^{4-}{}_{(aq)} \quad (2)$$

$$ZnC_2O_4 \cdot 2H_2O_{(solid)} = ZnC_2O_{4(solid)} + 2H_2O = Zn^{2+}{}_{(aq)} + C_2O_4{}^{2-}{}_{(aq)} + 2H_2O \quad (3)$$

$$MnC_2O_{4(solid)} = Mn^{2+}{}_{(aq)} + C_2O_4{}^{2-}{}_{(aq)} \quad (4)$$

$$C_2O_4{}^{2-}{}_{(aq)} + 2H^+{}_{(aq)} = 2CO_{2(gas)} + H_{2(gas)} \quad (5)$$

Yields were calculated by dividing experimental yields by theoretical yields assuming that Zn and Mn ions underwent conversion as $(Zn,Mn)_2SiO_4$. Theoretical mass of ZSM material that can be obtained from 100 mg of precursor is 49.8 mg.

The color of all products was white by visual examination in white light. Yields for reaction times below 5 min were over 100% because unreacted starting materials remained in the samples. These samples also showed large weight losses during TG-DTA measurements. For the product obtained at a reaction time of

Table 1
Analysis of Mn-doped zinc silicate produced by supercritical process

Run no.	Concentration of ZSM (mol/kg)	Reaction time (min)	Yield (%)	Weight loss (wt%)	Mn content (mol%)
1	0.30	1	172.3	43.5	2.1
2	0.30	2	154.6	43.1	1.7
3	0.30	3	130.4	29.1	1.4
4	0.30	4	121.7	25.1	1.6
5	0.30	5	109.7	24.3	1.6
6	0.30	10	94.1	5.2	2.2
7	0.30	30	94.8	3.4	2.5
8	0.30	90	92.7	0.7	1.8
9	0.30	180	88.3	0.4	2.3
10	0.30	4320	94.8	0.0	1.7
11	0.075	90	87.9	0.0	1.3
12	0.15	90	89.4	0.1	1.8
13	0.60	90	94.9	0.0	1.9

90 min, weight loss was under 1%, so that reactions at this time seemed to be complete.

XRD spectra and SEM images of products at various reaction times are given in Figs. 1 and 2, respectively. The precursor only had peaks associated with zinc oxalate dihydrate that was consistent with JCPDS No. 25-1029. The phase formation process can be interpreted with XRD spectra and the SEM images as follows. At a reaction time of 1 min, XRD spectrum (Fig. 1) showed that zinc oxalate dihydrate partially converted to zinc oxalate anhydrate which was consistent with JCPDS No. 37-0718. At 2 min, XRD spectrum (Fig. 1) showed that a small amount of zinc silicate phase appeared concurrently with α-phase (JCPDS No. 70-1235) and β-phase (JCPDS No. 19-1479), while it was not clear that the zinc silicate phase existed in the SEM image. At 3 min, the SEM image (Fig. 2) showed that needle-like particles having a length of 2 μm appeared that could be assigned to ZSM [25]. It seems that zinc silicate did not form on the surface of the silica particles, since the spherical silica particles shrank and supplied Si ions for the zinc silicate, while still maintaining their spherical shape. The present formation process is clearly different from the solid-state reaction where zinc silicate forms on the surface of silica [28,29]. At 4 (not shown) and 5 min (Fig. 1), XRD intensities of peaks attributed to α-ZSM and β-ZSM increased as reaction time progressed. At 10 min, XRD spectra (Fig. 1) showed that zinc oxalate dihydrate disappeared, while zinc oxalate anhydrate still existed slightly and $ZnCO_3$ (JCPDS No. 08-0449) appeared. It is an important problem on whether $ZnCO_3$ existed as a crystalline phase in supercritical water at these conditions or whether it precipitated as a crystalline phase after quenching. The SEM images showed that the spherical silica particles became smaller than those in the precursor. Solubility of silica in supercritical water at 400 °C and 30 MPa is about 0.06 wt% [30]. Silica seemed to decrease gradually with time as it was probably being consumed in the reaction. Existence of silica means that zinc ions did not react with silica, but they were probably present in the aqueous phase at 10 min. It is probable that Zn ions precipitated as an amorphous phase during quenching and partially formed as low-crystalline $ZnCO_3$. These precipitated Zn compounds appeared as irregularly shaped particles in the SEM images (Fig. 2). Thus, the formation of α-ZSM and β-ZSM probably increased with reaction time up until 10 min, while peaks attributed to β-ZSM decreased after 10 min reaction time. At 30 min, unreacted Zn ions still existed due to the presence of the XRD peaks assigned to $ZnCO_3$, and silica particles seemed to be present as observed in the SEM images. Further, the β-ZSM decreased considerably, while α-ZSM increased during this period. XRD spectra showed that α-ZSM phase mainly existed after 90 min reaction time and that α-ZSM single phase was completely formed after 4320 min (72 h) reaction time because of the disappearance of the peak assigned as β-ZSM phase near 36° (Fig. 1). It is reported that the most stable phase of zinc silicate is α-Zn_2SiO_4 at this temperature and pressure of the phase diagram [31]. SEM images (Fig. 2) at 90 and 180 min showed that the particles produced had two types of shapes, namely, needle-like shapes and irregular shapes. The needle-like-shaped particles were α-ZSM that were formed via a homogenous nucleation process [25]. The weight losses measured with TGA were essentially 0% so it is probable that the composition of particles produced was $(Zn,Mn)_2SiO_4$. Amorphous Zn_2SiO_4 is unknown, so the irregularly shaped particles were probably different shaped α-ZSM transformed from metastable β-ZSM via solid-state diffusion. The morphology of the α-ZSM and the transformation of β-ZSM into α-ZSM will be discussed further below. At 4320 min, the irregularly shaped particles disappeared. It seems that these irregularly shaped particles were unstable at the reaction conditions and they transformed into stable needle-like-shaped particles through dissolution in supercritical water and recrystallization at the long reaction times.

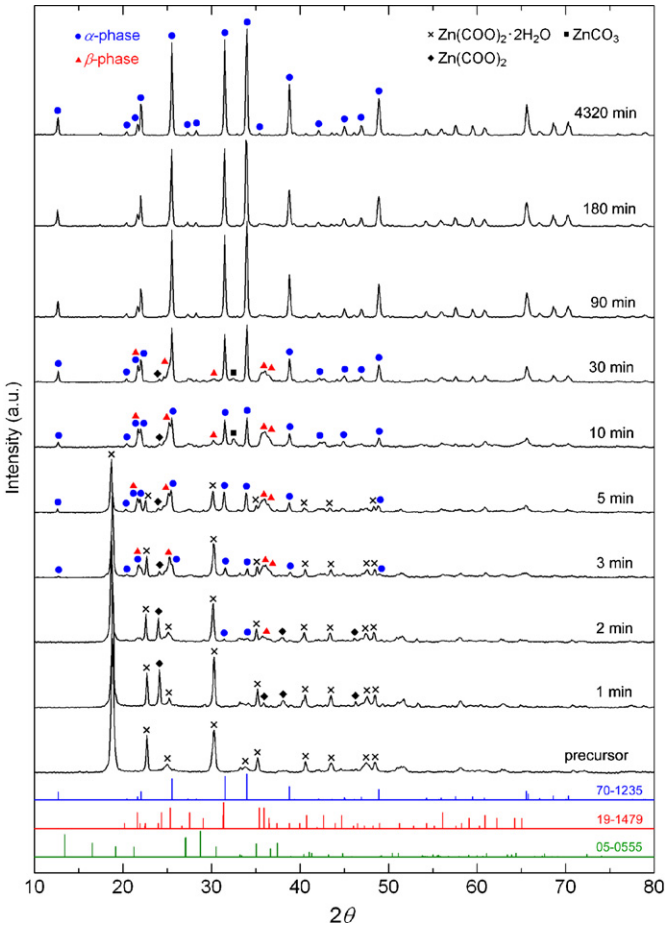

Fig. 1. XRD spectra of precursor and Mn-doped zinc silicate produced by supercritical process (400 °C, 29 MPa, 0.30 mol/kg) at reaction times from 1 to 4320 min. JCPDS no. 70-1235 (α-Zn_2SiO_4), 19-1479 (β-Zn_2SiO_4), and 05-0555 (hemimorphite) are shown as references.

It is reported that hemimorphite forms as an intermediate phase at conventional hydrothermal conditions [22]. From the XRD spectra (Fig. 1) hemimorphite, $Zn_4Si_2O_7(OH)_2 \cdot H_2O$ (JCPDS No. 05-0555) did not appear during the phase formation of ZSM at present conditions. Wan et al. reported that hemimorphite forms at temperatures from 160 to 240 °C in 1 h reaction time from precursor prepared from $ZnCl_2$ and Na_2SiO_3 aqueous solution [22]. Their experiments are probably carried out at a water density of about 0.6 g/cm^3, and thus at lower pressures of 0.7–3.5 MPa than this study. The reason why hemimorphite was not formed in this study is because the reaction rate of dehydrating metal salts is most likely faster than that of hydrolysis, especially since the present conditions of the system go through the critical region of water abruptly, where dehydration is promoted as opposed to hydration [32].

3.2. *Luminescence appearance of Mn-doped zinc silicate in supercritical water*

VUV-PL spectra of the produced ZSM are shown in Fig. 3. It is well known that α-ZSM has a green emission [4,6,7], while β-ZSM has a yellow emission [33–36]. Green and yellow emissions derived from Mn ions appear individually at a reaction time of 2 min when α-ZSM and β-ZSM formed slightly. Thus, through

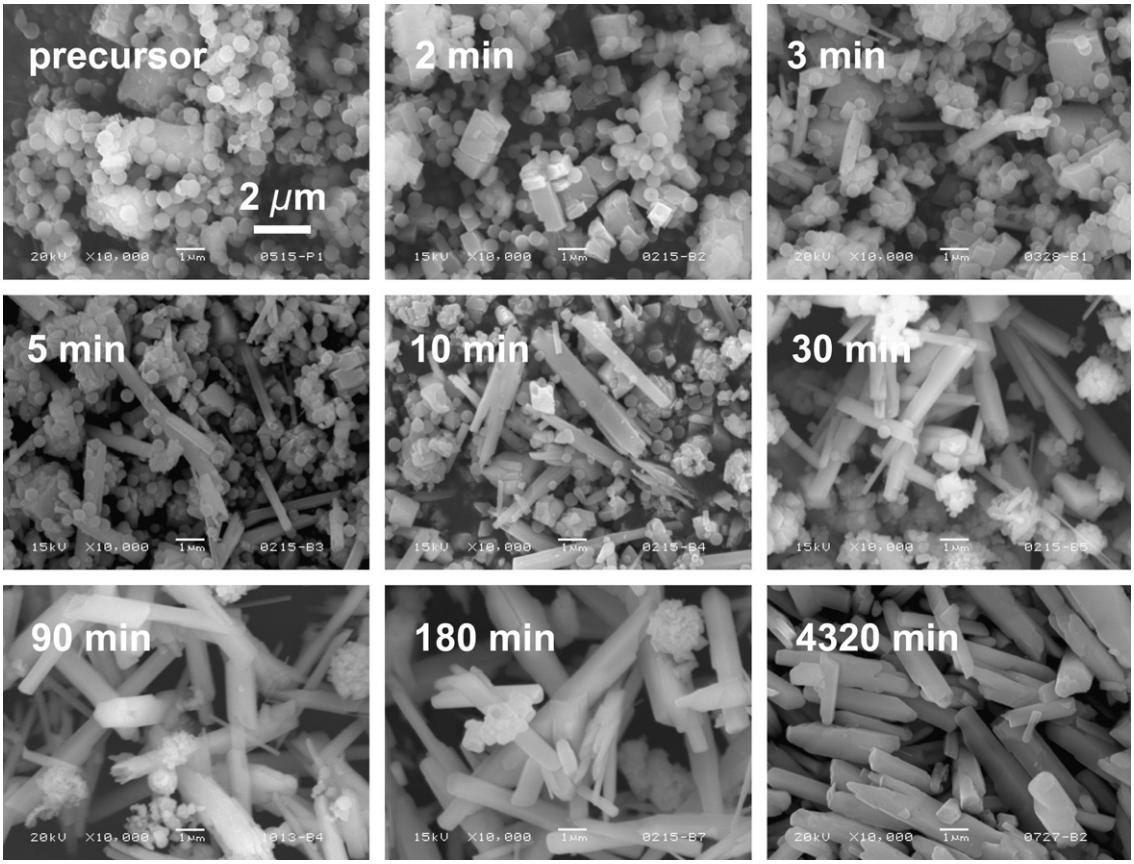

Fig. 2. SEM images of precursor and Mn-doped zinc silicate produced by supercritical process (400 °C, 29 MPa, 0.30 mol/kg) at reaction times from 2 to 4320 min.

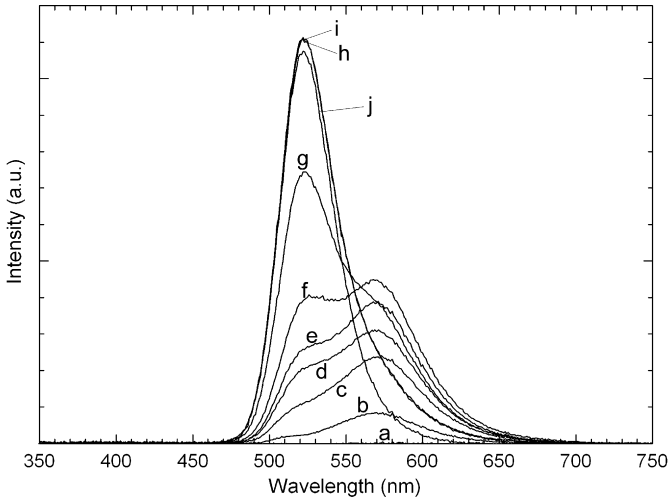

Fig. 3. VUV-PL spectra of Mn-doped zinc silicate produced by supercritical process (400 °C, 29 MPa, 0.30 mol/kg) at various reaction times: (a) 1 min, (b) 2 min, (c) 3 min, (d) 4 min, (e) 5 min, (f) 10 min, (g) 30 min, (h) 90 min, (i) 180 min, and (j) 4320 min.

reaction in supercritical water, luminescence appearance began at about the same time when ZSM phase formation could be recognized. The yellow emitting component (peak wavelength of about 570 nm) was stronger than the green emitting component (peak wavelength of about 525 nm) at reaction times shorter than 10 min, whereas the green emitting component became stronger at reaction times longer than 30 min. At a reaction time of 90 min, the yellow emission component decreased for the most part and the VUV-PL spectrum appeared asymmetric, which is typical for α-ZSM [37,38]. It should be noted that the green emission of α-ZSM synthesized by the supercritical process is based on the $^4T_1(^4G)\rightarrow{}^6A_1(^6S)$ transition of $3d^5$ electrons in the Mn^{2+} ion, which is the same as that for material synthesized by the solid-state reaction process.

A chromaticity coordinate diagram following CIE 1931 conventions is given in Fig. 4. The diagram shows that emission color varied continuously from yellow (2 min) to green (4320 min) as reaction time progressed. This time dependent behavior of emission color corresponded to the phase composition of α and β-phase that could be estimated from the XRD results. Yellow emission and green emission appeared individually and yellow emission changed to green emission without a color mixture (Fig. 3), reflecting each α-ZSM and β-ZSM phase that transformed independently. For the reaction time of 4320 min, the yellow emission component almost completely disappeared so that the dominant wavelength was located on the short wavelength side compared with that for commercial ZSM, 540 nm, which was calculated by the chromaticity coordinate (0.242, 0.708 [39]). This can be attributed to the stable α-phase, which formed as a stable shape that obeyed its crystal habit.

3.3. Phase transformation and particle shape of zinc silicate in supercritical water

Two different shapes of α-ZSM appeared at a reaction time of 90 min as noted previously. It seems probable that needle-like-shaped particles were formed via a homogenous nucleation process, while irregularly shaped particles were transformed from β-ZSM via solid-state diffusion. The needle-like-shaped ZSM

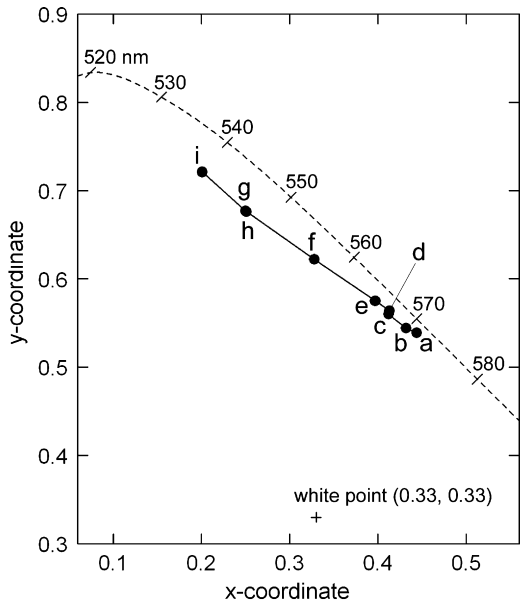

Fig. 4. Chromaticity coordinate diagram (following the CIE 1931) of Mn-doped zinc silicate produced by supercritical process (400 °C, 29 MPa, 0.30 mol/kg) at various reaction times: (a) 2 min, (b) 3 min, (c) 4 min, (d) 5 min, (e) 10 min, (f) 30 min, (g) 90 min, (h) 180 min, and (i) 4320 min. The dashed line is the spectrum locus.

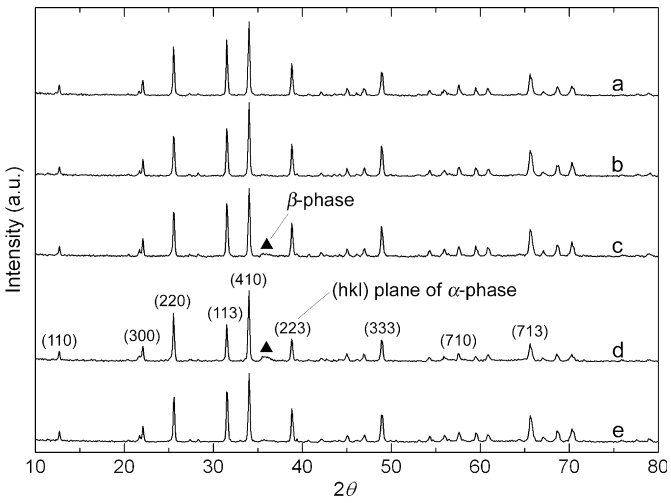

Fig. 5. XRD spectra of Mn-doped zinc silicate produced by supercritical process (400 °C, 29 MPa, 90 min) at various concentration: (a) 0.075 mol/kg, (b) 0.15 mol/kg, (c) 0.60 mol/kg, and XRD spectra after separation of the sample c: (d) upper layer after separation, (e) lower layer after separation.

particles have been observed to form at conditions close to the critical point of water [25].

Consider our previous results [25] and the results in this work, the formation mechanism of the irregularly shaped particles can be discussed. To compare concentrations at the reaction conditions, further experiments were performed at 0.075, 0.15, and 0.60 mol/kg and for a reaction time of 90 min at the same experimental conditions of temperature, loading, and starting materials. XRD spectra (Figs. 5a–c) of the products at a reaction time of 90 min showed that β-phase appeared only for the ZSM concentration of 0.60 mol/kg. SEM images (Figs. 6a–c) of the products at a reaction time of 90 min showed that many irregularly shaped particles were present at 0.60 mol/kg, but these were rarely seen at 0.075 mol/kg. Irregularly shaped particles and β-ZSM phase increased as concentration progressed at these conditions. Separation of irregularly shaped particles from the ZSM formed at concentration of 0.60 mol/kg and reaction time 90 min was carried out to see whether a relationship existed between irregularly shaped particles and β-ZSM phase.

The ZSM particles were dispersed in water with ultrasonication for a few minutes and allowed to stand so that particles separated into an upper layer (dispersed particles) and a lower layer (precipitated particles). Each layer was dried with an electric oven. The ZSM products before and after the separation were analyzed by XRD spectra (Figs. 5c–e), SEM images (Figs. 6c–e), and VUV-PL spectra (Fig. 7). VUV-PL spectra were normalized at the intensity of a peak wavelength of the green emitting component (523 nm) to allow relative comparisons between the ratio of the yellow emitting component to that of the green emitting component. XRD spectra (Fig. 6) showed that most of the β-phase existed in the upper layer involving more irregularly shaped particles after the separation. XRD intensities that were normalized at (410) plane showed that the intensities of (113), (223), and (333) planes of the upper layer after separation (Fig. 5d) were relatively higher than the intensities of the lower layer after separation, suggesting that a high proportion of the narrow needle-like-shaped particles existed in the lower layer as confirmed by the corresponding SEM image (Fig. 6d).

More interestingly, the VUV-PL spectra (Fig. 7a) showed that the upper layer after separation contained more yellow emitting component than in the mixture (Fig. 7c), whereas the lower layer exhibited less yellow emitting component (Fig. 7b). It is clear that the dominant wavelengths of the upper and lower layer were 548 and 537 nm, respectively. Thus, it is likely that the yellow emitting β-ZSM is contained in the irregularly shaped particles, and the irregularly shaped α-ZSM that appeared in the SEM images at 90 and 180 min reaction time (Fig. 2) was transformed from β-ZSM into α-ZSM. The transformation seems to be based on solid-state diffusion similar to that of the solid-state reaction, since the α-ZSM was not needle-like in shape, but rather had an irregular shape.

Distribution of Mn ions between the upper and lower layer in the ZSM particles will be discussed next. ICP-AES results indicated that the Mn contents of the upper and lower layer were 2.1 and 1.7 mol%, respectively. Mn ions were more distributed in the upper layer that contained relatively high amounts of irregularly shaped particles and β-ZSM than the lower layer. We previously reported that β-ZSM phase increased as Mn concentration progressed [25]. It seems that β-ZSM formed disproportionately near the Mn ion sites since solubility of manganese oxalate was higher than zinc oxalate dihydrate and anhydrate at these conditions.

Transformation of β-ZSM into α-ZSM is now discussed. In the solid-state reaction, it is well known that metastable β-ZSM forms at lower temperatures and this transforms into stable α-ZSM at higher temperatures [34–36,40]. Further, it has been reported that β-ZSM transforms into α-ZSM at temperatures of 919 °C [40] and 960 °C [35]. This transformation has no significant change in density and involves atomic rearrangement via solid-state diffusion [35]. The results presented in this study show that transformation of β-ZSM into α-ZSM occurs in supercritical water at a much lower temperature compared with the solid-state reaction, and transformation of irregularly shaped β-ZSM particles into α-ZSM was accompanied by no changes in the particle shape. If the transformation involved dissolution of β-ZSM and recrystallization of α-ZSM, the particle shape would probably have become needle-like, which is the same as α-ZSM generated through homogenous nucleation according to the crystal habit [41]. It is far more likely that the irregularly shaped β-ZSM transformed into irregularly shaped α-ZSM via solid-state diffusion much like the solid-state reaction. Thus, two shapes of α-ZSM that appeared at a reaction time of 90 min, those being needle-like

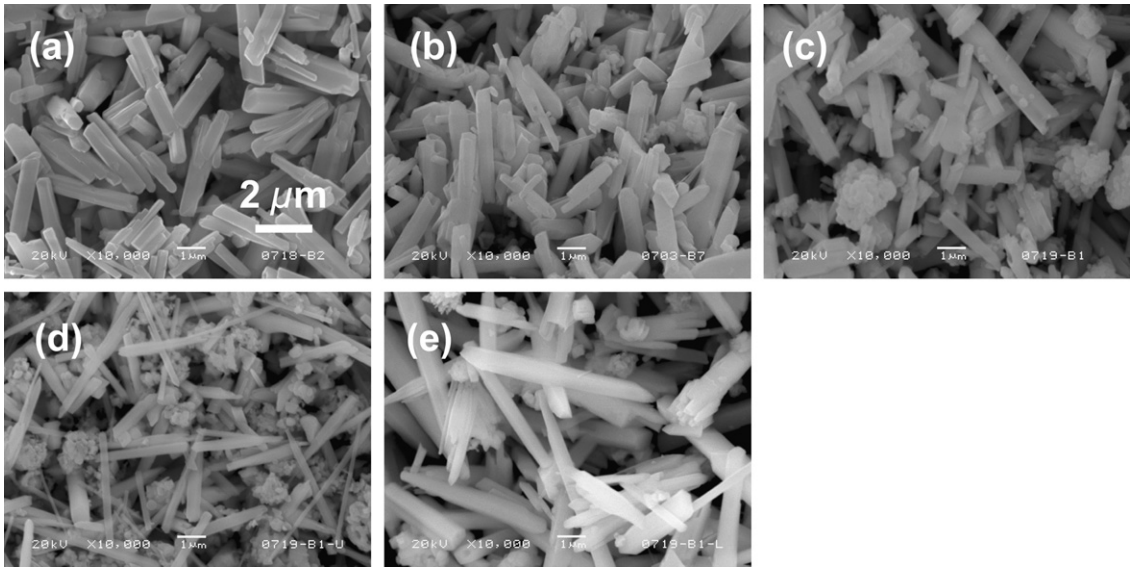

Fig. 6. SEM images of Mn-doped zinc silicate produced by supercritical process (400 °C, 29 MPa, 90 min) at various concentration: (a) 0.075 mol/kg, (b) 0.15 mol/kg, (c) 0.60 mol/kg, and SEM images after separation of the sample c: (d) upper layer after separation, (e) lower layer after separation.

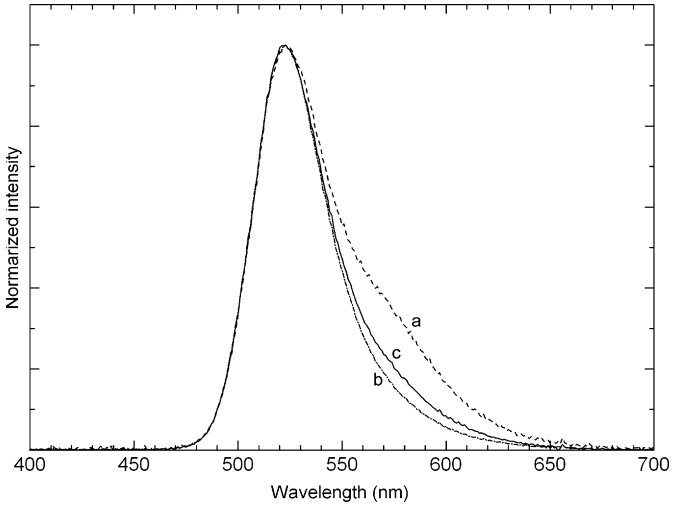

Fig. 7. VUV-PL spectra before and after separation of Mn-doped zinc silicate produced by supercritical process (400 °C, 29 MPa, 0.60 mol/kg, 90 min): (a) upper layer after separation, (b) lower layer after separation, and (c) before separation.

shapes and irregularly shapes that were different accordingly to their phase formation mechanism. Needle-like-shaped particles formed via homogenous nucleation in supercritical water, while irregularly shaped particles formed via solid-state diffusion among solid starting materials passing through metastable β-ZSM. It seems that irregularly shaped β-ZSM formed by diffusion of silica into insoluble zinc oxalate dihydrate and anhydrate, since spherical silica particles became smaller without changing the particle shape. Solubility of zinc oxalate dihydrate and anhydrate should be significantly lower in supercritical water compared to ambient conditions. This may be another reason why the amount of irregularly shaped β-ZSM particles increased as the concentration progressed.

Alteration of shape and phase transformation of ZSM in supercritical water is summarized by the species reactions:

$$(Zn, Mn)^{2+}{}_{(aq)} + SiO_4{}^{4-}{}_{(aq)} \rightarrow \text{needle } \alpha\text{-ZSM} \quad (6)$$

$$\text{Zn (Mn) oxalate compound}_{(solid)} + SiO_4{}^{4-}{}_{(aq)} \rightarrow \text{irregularly shaped } \beta\text{-ZSM} \quad (7)$$

$$\text{Irregularly shaped } \beta\text{-ZSM} \rightarrow \text{irregularly shaped } \alpha\text{-ZSM} \quad (8)$$

$$\text{Irregularly shaped } \alpha\text{-ZSM} \rightarrow \text{needle } \alpha\text{-ZSM} \quad (9)$$

The most stable shape and phase in supercritical water was needle-like-shaped α-ZSM that was formed via two probable routes. One route was homogenous nucleation from dissolved raw materials in supercritical water, producing needle-like-shaped α-ZSM particles from the first in one step (reaction (6)). The other routes (reactions (7)–(9)) were accompanied by the alteration of phase and shape stepwise. At first, irregularly shaped β-ZSM that formed on the surface of the Zn (Mn) oxalate compound (reaction (7)) that was probably a mixture of zinc oxalate dihydrate, zinc oxalate, and manganese oxalate. Next, metastable irregularly shaped α-ZSM particles transformed by atomic rearrangement based on solid-state diffusion of irregularly shaped β-ZSM (reaction (8)). Then, metastable α-ZSM particles were finally transformed into stable needle-like-shaped particles through dissolution in supercritical water and recrystallization after a sufficiently long reaction time (reaction (9)). The homogenous nucleation route probably began to dominate as the concentration of the starting materials decreased. The reason why the ZSM produced at lower concentration seldom contained β-phase and irregularly shaped particles as mentioned above is that the homogenous nucleation route probably dominates, since much zinc and manganese compounds are soluble at dilute conditions.

4. Conclusions

The most stable shape and phase of Mn-doped zinc silicate in supercritical water at 400 °C and 29 MPa was needle-like-shaped α-ZSM that was formed via two routes. One route was homogenous nucleation from dissolved raw materials in supercritical water, producing needle-like-shaped α-ZSM particles in one step.

The other route accompanied the transformation of β-ZSM into α-ZSM through solid-state diffusion and the alteration of shape through dissolution in supercritical water and recrystallization for long reaction time.

The luminescence appearance of ZSM as both green emission by α-ZSM and yellow emission by β-ZSM occurred over the same time period during the onset of phase formation. Luminescence appeared at a much lower temperature and at shorter reaction times than the conventional solid-state reaction. Emission color varied continuously from yellow to green as reaction time increased. The dominant wavelength of needle-like α-ZSM produced in supercritical water was located on the short wavelength side compared with that of commercial product. The results presented in this study show that the phase formation and luminescence of α-ZSM occurs in supercritical water at a much lower temperature compared to the solid-state reaction.

Acknowledgments

The authors wish to express their appreciation to Prof. Hajime Yamamoto (Tokyo University of Technology) for helpful discussion about luminescence properties.

References

[1] Y. Hakuta, H. Hayashi, K. Arai, Curr. Opin. Solid State Mater. Sci. 7 (2003) 341–351.
[2] E. Reverchon, R. Adami, J. Supercrit. Fluids 37 (2006) 1–22.
[3] C. Aymonier, A. Loppinet-Serani, H. Reverón, Y. Garrabos, F. Cansell, J. Supercrit. Fluids 38 (2006) 242–251.
[4] C.H. Lee, Y.C. Kang, K.Y. Jung, J.G. Choi, Mater. Sci. Eng. B117 (2005) 210–215.
[5] X. Wan, X.Y. Chen, Z.H. Wang, L. Mu, Y.T. Qian, J. Cryst. Growth 280 (2005) 239–243.
[6] A. Roy, S. Polarz, S. Rabe, B. Rellinghaus, H. Zahres, F.E. Kruis, M. Driess, Chem. Eur. J. 10 (2004) 1565–1575.
[7] H. Liang, Q. Zeng, Z. Tian, H. Lin, Q. Su, G. Zhang, Y. Fu, J. Electrochem. Soc. 154 (2007) J177–J180.
[8] H.X. Zhang, S. Buddhudu, C.H. Kam, Y. Zhou, Y.L. Lam, K.S. Wong, B.S. Ooi, S.L. Ng, W.X. Que, Mater. Chem. Phys. 68 (2001) 31–35.
[9] A. Patra, G.A. Baker, S.N. Baker, Opt. Mater. 27 (2004) 15–20.
[10] F.H. Su, B.S. Ma, K. Ding, G.H. Li, S.P. Wang, W. Chen, A.G. Joly, D.E. McCready, J. Lumin. 116 (2006) 117–126.
[11] A.G. Joly, W. Chen, J. Zhang, S. Wang, J. Lumin. 126 (2007) 491–496.
[12] V. Natarajan, K.V.R. Murthy, M.L.J. Kumar, Solid State Commun. 134 (2005) 261–264.
[13] Q.Y. Zhang, K. Pita, C.H. Kam, J. Phys. Chem. Solids 64 (2004) 333–338.
[14] H.M. Yang, J.X. Shi, M.L. Gong, J. Mater. Sci. 40 (2005) 6007–6010.
[15] T.S. Copeland, B.I. Lee, J. Qi, A.K. Elrod, J. Lumin. 97 (2002) 168–173.
[16] R.P. Sreekanth Chakradhar, B.M. Nagabhushana, G.T. Chandrappa, K.P. Ramesh, J.L. Rao, J. Chem. Phys. 121 (2004) 10250–10259.
[17] J. Xu, E.S. O'Keefe, C.C. Perry, J. Mater. Chem. 14 (2004) 1744–1748.
[18] Q.H. Li, S. Komarneni, R. Roy, J. Mater. Sci. 30 (1995) 2358–2363.
[19] T.S. Ahmadi, M. Haase, H. Weller, Mater. Res. Bull. 35 (2000) 1869–1879.
[20] S.W. Lu, T. Copeland, B.I. Lee, W. Tong, B.K. Wagner, W. Park, F. Zhang, J. Phys. Chem. Solids 62 (2001) 777–781.
[21] C. Yoon, S. Kang, J. Mater. Res. 16 (2001) 1210–1216.
[22] H. Wang, Y. Ma, G. Yi, D. Chen, Mater. Chem. Phys. 82 (2003) 414–418.
[23] J.X. Wan, Z.H. Wang, X.Y. Chen, L. Mu, W.C. Yu, Y.T. Qian, J. Lumin. 121 (2006) 32–38.
[24] T. Miki, T. Ogawa, T. Isobe, H. Sfihi, J. Sol–Gel Sci. Technol. 31 (2004) 73–77.
[25] M. Takesue, K. Shimoyama, S. Murakami, Y. Hakuta, H. Hayashi, R.L. Smith Jr., J. Supercrit. Fluids 43 (2007) 214–221.
[26] Z. Fang, R.L. Smith Jr., H. Inomata, K. Arai, J. Supercrit. Fluids 16 (2000) 207–216.
[27] T. Wang, R.L. Smith Jr., H. Inomata, K. Arai, Hydrometallurgy 65 (2002) 159–175.
[28] D.E. Harrison, J. Electrochem. Soc. 107 (1960) 210–217.
[29] S. Onodera, Mater. Res. Bull. 31 (1996) 793–796.
[30] J.V. Walther, H.C. Helgeson, Am. J. Sci. 277 (1977) 1315–1351.
[31] Y. Syono, S. Akimoto, Y. Matsui, J. Solid State Chem. 3 (1971) 369–380.
[32] T. Yamaguchi, M. Yamagami, H. Ohzono, H. Wakita, K. Yamanaka, Chem. Phys. Lett. 252 (1996) 317–321.
[33] H.P. Rooksby, A.H. McKeag, Trans. Faraday Soc. 37 (1941) 308–311.
[34] H.W. Leverenz, Science 109 (1949) 183–195.
[35] H.F.W. Taylor, Am. Mineral. 47 (1962) 932–944.
[36] N. Taghavinia, G. Lerondel, H. Makino, A. Yamamoto, T. Yao, Y. Kawazoe, T. Goto, Nanotechnology 12 (2001) 547–551.
[37] C.C. Klick, J.H. Schulman, J. Opt. Soc. Am. 42 (1952) 910–916.
[38] A.L.N. Stevels, A.T. Vink, J. Lumin. 8 (1974) 443–451.
[39] C.R. Ronda, J. Lumin. 72-74 (1997) 49–54.
[40] C.-C. Lin, P. Shen, J. Solid State Chem. 112 (1994) 387–391.
[41] K. Kodaira, S. Ito, T. Matsushita, J. Cryst. Growth 29 (1975) 123–124.